Collective *P*-Wave Orbital Dynamics of Ultracold Fermions

Mikhail Mamaev [ORCID],[1,2,*] Peiru He,[1,2] Thomas Bilitewski [ORCID],[1,2] Vijin Venu,[3] Joseph H. Thywissen,[3] and Ana Maria Rey [ORCID][1,2]

[1]*JILA, NIST, and Department of Physics, University of Colorado, Boulder, Colorado 80309, USA*
[2]*Center for Theory of Quantum Matter, University of Colorado, Boulder, Colorado 80309, USA*
[3]*Department of Physics and CQIQC, University of Toronto, Ontario M5S 1A7, Canada*

We consider the nonequilibrium orbital dynamics of spin-polarized ultracold fermions in the first excited band of an optical lattice. A specific lattice depth and filling configuration is designed to allow the p_x and p_y excited orbital degrees of freedom to act as a pseudospin. Starting from the full Hamiltonian for p-wave interactions in a periodic potential, we derive an extended Hubbard-type model that describes the anisotropic lattice dynamics of the excited orbitals at low energy. We then show how dispersion engineering can provide a viable route to realizing collective behavior driven by p-wave interactions. In particular, Bragg dressing and lattice depth can reduce single-particle dispersion rates, such that a collective many-body gap is opened with only moderate Feshbach enhancement of p-wave interactions. Physical insight into the emergent gap-protected collective dynamics is gained by projecting the Hamiltonian into the Dicke manifold, yielding a one-axis twisting model for the orbital pseudospin that can be probed using conventional Ramsey-style interferometry. Experimentally realistic protocols to prepare and measure the many-body dynamics are discussed, including the effects of band relaxation, particle loss, spin-orbit coupling, and doping.

Introduction.—Ultracold quantum gases in optical lattices are among the leading platforms for quantum simulation of strongly correlated matter and nonequilibrium dynamics. While there has been impressive experimental progress [1,2], most investigations thus far have been limited to *s*-wave interacting systems in the lowest motional band. A fascinating avenue yet to be explored experimentally is many-body lattice physics with *p*-wave interactions [3,4] in higher bands. *P*-wave interacting systems can host long-sought phases, including topological superfluids, Majorana fermions [5–7], and itinerant ferromagnetism [8–12]. At the same time, atoms in higher bands are a unique resource [13] for emulating orbital degrees of freedom in real materials [14] that give rise to heavy fermions [15], Ruderman-Kittel–Kasuya-Yosida interactions [16], and orbitally ordered Mott phases [17,18].

Despite these attractive features, control and manipulation of *p*-wave interacting gases has remained a challenge for ultracold atom experiments. The timescales on which *p*-wave interactions contribute to dynamics tend to be slow compared to coherence times [19] and lossy when increased by a Feshbach resonance [20–22]. Moreover, collisions in higher bands suffer from band relaxation [23,24]. Important progress in mitigating relaxation has been made via designed lattice geometries [25–27] and symmetry protection [28], but further advances are required to explore the full range of orbital physics in optical lattices.

Here, we consider the problem of nonequilibrium orbital physics in an optical lattice and identify a limit in which collective dynamics emerge. Orbital dynamics in the first excited bands are stabilized via Pauli blocking by preparing a spin-polarized system with a completely filled ground band, mimicking the conventional conduction-band configuration of materials. *P*-wave interactions are enabled by the orbitally antisymmetric two-atom wave functions. We explore the use of Bragg dressing to suppress orbital anisotropy, which allows an accurate mapping of the *p*-wave Fermi-Hubbard model to an *XXZ* spin model in which the conventional magnetic spin states are replaced by orbital states. We delineate a specific regime in which the collective dynamics can be further mapped to a collective one-axis twisting (OAT) model thanks to the opening of a many-body gap [29]. Dispersion engineering lowers the demands on Feshbach-tuned interaction strength, and thus elastic interactions can dominate over inelastic collisions and other decoherence processes. We further discuss how the *p*-wave induced mean-field dynamics can be observed with a Ramsey protocol.

The conceptual map that we develop offers new ways to understand *p*-wave orbital physics in an experimentally accessible regime. We connect previously established real-space pseudopotential formulations to a tractable extended Fermi-Hubbard model and use laser driving as a tool to coordinate interaction-driven dynamics. We show that a simple collective model can explain the emergent gap-protected dynamics.

P-wave Fermi-Hubbard model.—The scenario we consider is a three-dimensional (3D) optical lattice loaded with spin-polarized fermionic atoms in their ground electronic

state. The system Hamiltonian can be written in terms of field operators $\hat{\psi}(\vec{R})$ acting in real space $\vec{R} = (X, Y, Z)$ as

$$\hat{H} = \int d^3\vec{R}\hat{\psi}^\dagger \left[-\frac{\hbar^2}{2m}\vec{\nabla}^2 + \sum_{\nu=X,Y,Z} V_\nu E_r \sin^2\left(\frac{\pi\nu}{a}\right) \right]\hat{\psi}$$
$$- \sum_{\nu=X,Y,Z} \frac{3\pi\hbar^2 b_\nu^3}{2m} \int d^3\vec{R} W_\nu(\hat{\psi}^\dagger, \hat{\psi}^\dagger) W_\nu(\hat{\psi}, \hat{\psi}), \quad (1)$$

where $W_\nu(\hat{A}, \hat{B}) = (\vec{\nabla}_\nu \hat{A})\hat{B} - \hat{A}(\vec{\nabla}_\nu \hat{B})$. The first line includes the kinetic energy and lattice potential, where the lattice depth along $\nu \in \{X, Y, Z\}$ is $V_\nu E_r$ with E_r the recoil energy, a is the lattice spacing and m is the atomic mass. We assume that $V_X = V_Y \ll V_Z$, confining the system to independent 2D planes. The second line contains the collisional interactions, which are p-wave since the s-wave channel is blocked for a spin-polarized gas. We have used a pseudopotential approximation [30–33] with two different scattering volumes due to dipole-dipole splitting of the closed channel, $b_X^3 = b_Y^3 \equiv b_{XY}^3$ and b_Z^3, controlled by a p-wave Feshbach resonance. We assume a magnetic field pointed along the tight confined direction Z; for such a field, we will show that only the transverse volume b_{XY}^3 is relevant for the interactions that our specific configuration will exhibit. We also note that while the p-wave scattering volume tends to have strong energy dependence, we operate in the regime where the energy dependence can be well approximated as an additional constant shift in the position of the Feshbach resonance [34].

We seek to work in the ultracold regime where atoms only occupy the ground band and the first excited bands of the X and Y directions, with orbitals $\phi_{\vec{r}}^\gamma(\vec{R})$ given by

$$\phi_{\vec{r}}^g(\vec{R}) = w_0^X(X - ia)w_0^Y(Y - ja)w_0^Z(Z),$$
$$\phi_{\vec{r}}^\Uparrow(\vec{R}) = w_1^X(X - ia)w_0^Y(Y - ja)w_0^Z(Z), \quad \text{and}$$
$$\phi_{\vec{r}}^\Downarrow(\vec{R}) = w_0^X(X - ia)w_1^Y(Y - ja)w_0^Z(Z), \quad (2)$$

where $\vec{r} = \{ia, ja\}$ is the lattice position on the 2D plane, $\gamma \in \{g, \Uparrow, \Downarrow\}$ is the band index, and $w_n^\nu(\nu - ia)$ is the nth lattice Wannier function localized at site i of direction ν. Our desired configuration is a filling of $N/L = 2$: each site will have one atom in the g orbital, filling the ground band, and a second atom in the degenerate subspace of the excited orbitals $\{\Uparrow, \Downarrow\}$ acting as a spin-1/2 degree of freedom. The occupation of the ground state prevents collisional relaxation since, for any energy-conserving two-atom process, leaving the excited subspace would require an atom to move down to the ground band; here, this is forbidden by Pauli exclusion.

The low-energy Hamiltonian can be written as an anisotropic multiorbital model by projecting $\hat{H}$ into the Wannier basis defined by the three chosen orbital states, yielding

$$\hat{H}_{\rm FH} = \hat{H}_J + \hat{H}_{\rm int}. \quad (3)$$

Here, $\hat{H}_J$ describes the kinetic energy of the excited atoms, which tunnel to nearest neighbor sites at rate J_0 or J_1 depending on the tunneling direction and orbital: the $\Uparrow$ atoms tunnel at rate J_1 along X and rate J_0 along Y, while the $\Downarrow$ atoms do the opposite [see Fig. 1(a)]. In general $J_1 \gg J_0$ since excited states have a larger spatial extent along their excitation direction. Since the g atoms are in a filled band, they are Pauli blocked and do not contribute to $\hat{H}_J$. For the excited atoms, the tunneling Hamiltonian can be written in momentum space as

$$\hat{H}_J = \sum_{\vec{k}} \epsilon_{\vec{k}}(\hat{n}_{\vec{k},\Uparrow} - \hat{n}_{\vec{k},\Downarrow}) + \sum_{\vec{k}} \bar{E}_{\vec{k}}(\hat{n}_{\vec{k},\Uparrow} + \hat{n}_{\vec{k},\Downarrow}), \quad (4)$$

with $\epsilon_{\vec{k}} = (J_1 + J_0)[\cos(k_X a) - \cos(k_Y a)]$ and $\bar{E}_{\vec{k}} = (J_1 - J_0)[\cos(k_X a) + \cos(k_Y a)]$. Here, $\hat{n}_{\vec{k},\gamma} = \hat{c}_{\vec{k},\gamma}^\dagger \hat{c}_{\vec{k},\gamma}$ and $\hat{c}_{\vec{k},\gamma} = L^{-1/2} \sum_{\vec{r}} e^{i\vec{r}\cdot\vec{k}}\hat{c}_{\vec{r},\gamma}$, with $\vec{k} = (k_X, k_Y)$ the lattice quasimomentum and $\hat{c}_{\vec{r},\gamma}$ annihilating an atom on lattice site $\vec{r}$ in band state $\gamma \in \{\Uparrow, \Downarrow\}$.

The second term $\hat{H}_{\rm int}$ contains the interactions. Using the Wannier expansion, these take the form of

$$\hat{H}_{\rm int} \approx \sum_{\vec{r},\vec{r}',\vec{r}'',\vec{r}'''} \sum_{\alpha,\beta,\sigma,\gamma} U_{\vec{r},\vec{r}',\vec{r}'',\vec{r}'''}^{\alpha\beta\sigma\gamma} \hat{c}_{\vec{r},\alpha}^\dagger \hat{c}_{\vec{r}',\beta}^\dagger \hat{c}_{\vec{r}'',\sigma} \hat{c}_{\vec{r}''',\gamma},$$

$$U_{\vec{r},\vec{r}',\vec{r}'',\vec{r}'''}^{\alpha\beta\sigma\gamma} = G^{XY} \sum_{\nu=X,Y} \int d^3\vec{R} W_\nu(\phi_{\vec{r}}^{\alpha*}, \phi_{\vec{r}'}^{\beta*}) W_\nu(\phi_{\vec{r}''}^\sigma, \phi_{\vec{r}'''}^\gamma),$$

$$(5)$$
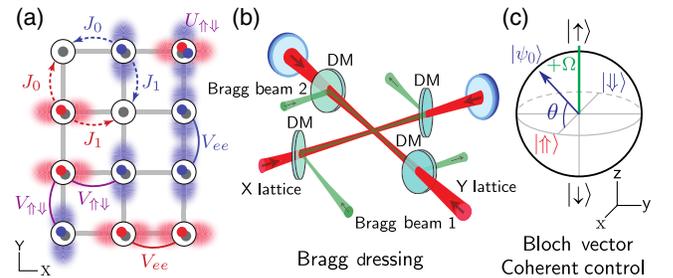

FIG. 1. Conceptual schematic. (a) Fermi-Hubbard physics on a single X-Y plane. The $\Uparrow$ (X-excited) and $\Downarrow$ (Y-excited) atoms tunnel at rates J_0 and J_1 along their ground and excited directions, respectively. There is an on-site p-wave interaction $U_{\Uparrow\Downarrow}$ between $\Uparrow$, $\Downarrow$ atoms, as well as nearest-neighbor interactions V_{ee}, $V_{\Uparrow\Downarrow}$. (b) Bragg dressing coupling $\Uparrow$, $\Downarrow$ can be implemented with beams (shown in green) that copropagate with the lattice beams (red) when the Bragg-laser wavelength is half that of the lattice beams. The out-of-plane lattice beam is not shown. (c) Effective Bloch sphere of the Bragg-dressed spin states. The $\Uparrow$, $\Downarrow$ states are equal superpositions of the two flavors of the dressed basis. Using standard coherent control protocols, any direction of the Bloch vector can be initialized.

where $G^{XY} = -[(3\pi\hbar^2 b_{XY}^3)/2m]$, $\{\vec{r}, \vec{r}', \vec{r}'', \vec{r}'''\}$ each run over all lattice sites and $\{\alpha, \beta, \sigma, \gamma\}$ over band states $\{g, \Uparrow, \Downarrow\}$. Since all included orbitals have the same wave function along the Z direction and we assume tight confinement V_Z restricting the system to 2D planes, only contributions from the terms proportional to the transverse volume b_{XY}^3 are relevant.

We evaluate all these terms and keep the ones that have non-negligible coefficient $U_{\vec{r},\vec{r}',\vec{r}'',\vec{r}'''}^{\alpha\beta\sigma\gamma}$ on realistic timescales and are not inhibited by a band gap or another stronger interaction [34]. For a sufficiently deep lattice $V_X = V_Y \gg 1$ the relevant terms give rise to an extended Fermi-Hubbard model that consists of on-site (OS) and nearest-neighbor (NN) interactions, $\hat{H}_{\text{int}} = \hat{H}_{\text{int}}^{(\text{OS})} + \hat{H}_{\text{int}}^{(\text{NN})}$. The on-site term is

$$\hat{H}_{\text{int}}^{(\text{OS})} \approx U_{\Uparrow\Downarrow} \sum_{\vec{r}} \hat{n}_{\vec{r},\Uparrow} \hat{n}_{\vec{r},\Downarrow}, \qquad (6)$$

corresponding to a density-density interaction between $\Uparrow$ and $\Downarrow$ atoms with strength $U_{\Uparrow\Downarrow} = 4U_{\vec{r},\vec{r},\vec{r},\vec{r}}^{\Uparrow\Downarrow\Downarrow\Uparrow}$. On-site interactions between $\Uparrow$, g and between $\Downarrow$, g are also present but amount to a constant of motion for $V_X = V_Y$ and can be dropped. The nearest-neighbor terms are anisotropic density-density interactions given by

$$\hat{H}_{\text{int}}^{(\text{NN})} \approx V_{ee} \sum_{\vec{r}} \left(\hat{n}_{\vec{r},\Uparrow} \hat{n}_{\vec{r}+\vec{r}_X,\Uparrow} + \hat{n}_{\vec{r},\Downarrow} \hat{n}_{\vec{r}+\vec{r}_Y,\Downarrow} \right)$$
$$+ V_{\Uparrow\Downarrow} \sum_{\vec{r},\nu=X,Y} \left(\hat{n}_{\vec{r},\Uparrow} \hat{n}_{\vec{r}+\vec{r}_\nu,\Downarrow} + \hat{n}_{\vec{r},\Downarrow} \hat{n}_{\vec{r}+\vec{r}_\nu,\Uparrow} \right). \qquad (7)$$

Here, $\vec{r}_\nu$ is a lattice unit vector along the $\nu \in \{X, Y\}$ direction. The interaction $V_{ee} = 4U_{\vec{r},\vec{r}+\vec{r}_X,\vec{r}+\vec{r}_X,\vec{r}}^{\Uparrow\Uparrow\Uparrow\Uparrow}$ is between nearest-neighbor pairs of atoms in the same excited orbital along their excitation direction, as depicted in Fig. 1(a). $V_{\Uparrow\Downarrow} = 4U_{\vec{r},\vec{r}+\vec{r}_X,\vec{r}+\vec{r}_X,\vec{r}}^{\Uparrow\Downarrow\Downarrow\Uparrow}$ is an interaction between nearest neighbor atoms in different excited orbitals. For a sample atom choice of ^{40}K and parameters of $V_X = V_Y = 25$, $V_Z = 100$, $b_{XY} = 292 a_0$ with a_0 the Bohr radius (a 20-fold increase in background volume), we predict coefficients of $J_0 = 5$ Hz, $J_1 = 130$ Hz, $U_{\Uparrow\Downarrow} = 900$ Hz, $V_{ee} = 0.3$ Hz, and $V_{\Uparrow\Downarrow} = 0.1$ Hz. These parameters are used in the following calculations, unless otherwise specified.

Momentum-space spin model.—The implementation of an anisotropic extended Fermi-Hubbard model, Eq. (3), already offers exciting opportunities for quantum simulation [37]. However, as a first step we are specifically interested in regimes amenable for theoretical analysis, starting from a fully polarized initial state, where nevertheless p-wave interactions play a dominant role. For our p-wave system, however, the large spin dependent dispersion in $\hat{H}_J$ will induce fast single particle dynamics

that quickly depolarizes the initial state. To favor ordering of the orbital states, one can reduce competitive depolarization via the introduction of a laser field that couples $\Uparrow$ and $\Downarrow$:

$$\hat{H}_\Omega = \frac{\Omega}{2} \sum_{\vec{k}} \left(\hat{c}_{\vec{k},\Uparrow}^\dagger \hat{c}_{\vec{k},\Downarrow} + \text{H.c.} \right). \qquad (8)$$

Experimentally, such a term can be generated by an optical field whose Bragg grating is oriented along a diagonal reciprocal lattice vector [see Fig. 1(b)]. We assume that the drive couples only atoms with equal quasimomentum, which can be ensured with appropriate laser wavelengths and orientation [34]. Dressed with this coupling, the single-particle eigenenergies $E_{\vec{k}}^\pm$ of the atoms change from $\bar{E}_{\vec{k}} \pm \epsilon_{\vec{k}}$ to $\bar{E}_{\vec{k}} \pm \sqrt{\epsilon_{\vec{k}}^2 + (\Omega/2)^2}$. When $\Omega/2 \gg |\epsilon_{\vec{k}}|$, the anisotropic part of the spectrum $\epsilon_{\vec{k}}$ is flattened, which allows interactions to play a more dominant role in the spin dynamics.

Under the assumption of a strong drive $\Omega/2 \gg |\epsilon_{\vec{k}}|$, the flattened spectrum suppresses quasi-momentum-changing collisions between the atoms, which renders each atom frozen in a given $\vec{k}$ mode when evolving from a collective initial product state. In this regime, also known as the collisionless regime [38,39], we can approximate the Fermi-Hubbard model with a spin-1/2 model $\hat{H}_{\text{FH}} + \hat{H}_\Omega \approx \hat{H}_S$:

$$\hat{H}_S = \sum_{\vec{k},\vec{k}'} U_{\vec{k},\vec{k}'} \vec{\sigma}_{\vec{k}} \cdot \vec{\sigma}_{\vec{k}'} + \sum_{\vec{k},\vec{k}'} V_{\vec{k},\vec{k}'} \hat{\sigma}_{\vec{k}}^x \hat{\sigma}_{\vec{k}'}^x + \sum_{\vec{k}} \left(\epsilon_{\vec{k}} \hat{\sigma}_{\vec{k}}^x + \frac{\Omega}{2} \hat{\sigma}_{\vec{k}}^z \right),$$

with coefficients

$$U_{\vec{k},\vec{k}'} = -\frac{U_{\Uparrow\Downarrow}}{4L} - \frac{V_{\Uparrow\Downarrow}}{2L} [\cos(k_X a - k_X' a) + \cos(k_Y a - k_Y' a)],$$
$$V_{\vec{k},\vec{k}'} = \frac{V_{ee} - 2V_{\Uparrow\Downarrow}}{4L} [2 - \cos(k_X a - k_X' a) - \cos(k_Y a - k_Y' a)].$$

Here, we define spin operators $\hat{\sigma}_{\vec{k}}^\alpha = \hat{a}_{\vec{k},\mu}^\dagger \sigma_{\mu\mu'}^\alpha \hat{a}_{\vec{k},\mu'}$, σ^α the standard 2×2 Pauli matrices for $\alpha \in \{x, y, z\}$, summing over new dressed atom flavors $\mu, \mu' \in \{\uparrow, \downarrow\}$ that are eigenstates of the drive [see Fig. 1(c)]:

$$\hat{a}_{\vec{k},\uparrow} = \frac{1}{\sqrt{2}} (\hat{c}_{\vec{k},\Uparrow} + \hat{c}_{\vec{k},\Downarrow}) \quad \text{and} \quad \hat{a}_{\vec{k},\downarrow} = \frac{1}{\sqrt{2}} (\hat{c}_{\vec{k},\Uparrow} - \hat{c}_{\vec{k},\Downarrow}). \qquad (9)$$

The on-site contribution proportional to $U_{\Uparrow\Downarrow}$ is SU(2) symmetric, because only the orbital singlet state of the two excited bands can interact, while the nearest-neighbor terms yield XXZ-type anisotropicity.

Ramsey spectroscopy.—To probe the system dynamics, we consider the time evolution of a collective product state

$$|\psi_0\rangle = e^{i\theta\hat{S}^y}\prod_{\vec{k}}|\rightarrow\rangle_{\vec{k}}, \qquad (10)$$

where $|\rightarrow\rangle_{\vec{k}} = (|\uparrow\rangle_{\vec{k}} + |\downarrow\rangle_{\vec{k}})/\sqrt{2}$ is an X-excited ($\Uparrow$) band state and $\hat{S}^{\alpha=x,y,z} = \frac{1}{2}\sum_{\vec{k}}\hat{\sigma}_{\vec{k}}^{\alpha=x,y,z}$ are collective-spin operators. This state corresponds to either all spins pointing along the x direction of the dressed Bloch sphere, or inclined at some angle θ into the x-z plane [see Fig. 1(c)]. Such a state can be prepared from a band insulator by using Raman coupling schemes and control over the lattice depth [34]. We still assume ideal filling of 2 atoms per site, although a small hole fraction can be tolerated [34].

To probe the dynamics of this initial state, we propose a Ramsey-style protocol. The system is initialized and evolved for a time $t/2$ under the full Hamiltonian. The sign of the drive is then quenched from $+\Omega \rightarrow -\Omega$ with, e.g., a fast pulse of the laser detuning, and the system is evolved for another time $t/2$, undoing the drive's single-particle rotation. Then the collective observable $\langle\hat{S}^+\rangle = \langle\hat{S}_x\rangle + i\langle\hat{S}_y\rangle \equiv C(t)e^{i\phi(t)}$ is measured where $C = (\langle\hat{S}^x\rangle^2 + \langle\hat{S}^y\rangle^2)^{1/2}$ is the contrast, and $\phi = \arg\langle\hat{S}^+\rangle$ an interaction-induced phase shift.

Measurements of such collective-spin observables are straightforward to implement as the excited bands have different spatial distributions upon being released from the lattice. Turning off both the drive and the lattice and measuring the resulting gas cloud's X-band population ($\Uparrow$) via band-mapping [40] allows measurements of $\langle\hat{S}^x\rangle$. Leaving the drive on for an additional time $t\Omega = \pi/2$ after the Ramsey protocol rotates y into x, allowing the measurement of $\langle\hat{S}^y\rangle$ via an $\langle\hat{S}^x\rangle$ measurement. While $\langle\hat{S}^z\rangle$ is in principle conserved for $\Omega/2 \gg |\epsilon_{\vec{k}}|$, we can also measure it by advancing the relative phase of the Bragg beams ahead by $\pi/2$, which allows us to use the drive for a $\pi/2$ pulse that rotates z into x and then measuring $\langle\hat{S}^x\rangle$ once more.

Figures 2(a),(b) show the single-particle spectrum $E_{\vec{k}}^{\pm}$ and representative time evolution of the contrast for both the driven Fermi-Hubbard model $\hat{H}_{\text{FH}} + \hat{H}_{\Omega}$ and the spin model $\hat{H}_S$, starting from $|\psi_0\rangle$ and setting $\theta = 0$. Panel (a) corresponds to the case of a weak drive $\Omega/2 \lesssim |\epsilon_{\vec{k}}|$ and (b) to the case of a strong drive $\Omega/2 \gg |\epsilon_{\vec{k}}|$. We see a characteristic crossover from fast single-particle dynamics to a slow collective interaction-induced decay. To more clearly identify these regimes and benchmark our spin model mapping, we compare the time evolution of the two models in Fig. 2(c) with a root-mean-square error of the contrast. The spin model is valid when either the lattice depth is very shallow and single-particle tunneling dominates, or when the drive is strong enough to flatten the spectrum and make the single-particle dispersion
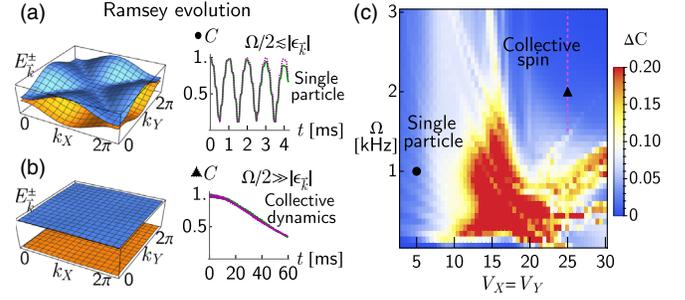

FIG. 2. (a),(b) Single-particle spectrum $E_{\vec{k}}^{\pm} = \bar{E}_{\vec{k}} \pm \sqrt{\epsilon_{\vec{k}}^2 + (\Omega/2)^2}$ and characteristic contrast time evolution for (a) a weak drive $\Omega/2 \lesssim |\epsilon_{\vec{k}}|$ and (b) a strong drive $\Omega/2 \gg |\epsilon_{\vec{k}}|$ for the Fermi-Hubbard+drive model $\hat{H}_{\text{FH}} + \hat{H}_{\Omega}$ (green) and spin model $\hat{H}_S$ (purple). (c) Benchmark comparison of the two models' agreement. Both models are evolved from a product state $|\psi_0\rangle$ with $\theta = 0$ to a fixed time $t_f = 50/J_1$, and their contrast C is compared with a root-mean-square error $\Delta C = [(1/t_f)\int_0^{t_f} dt |(2/L)(C_S - C_{\text{FH}+\Omega})|^2]^{1/2}$, truncated to $\min(\Delta C, 0.2)$ for clarity, using a small system $L = 3 \times 3$. The representative evolutions in panels (a),(b) are indicated by the circle and triangle, respectively. The purple dashed line indicates the collective regime explored further in Fig. 3.

subdominant with respect to the p-wave exchange interactions. At this point, a many-body gap energetically suppresses single-particle dynamics and keeps the spins aligned, allowing for collective behavior [29,41].

One-axis twisting.—When in the collective, gap-protected regime, the dominant spin model terms are the Heisenberg term $-(U_{\Uparrow\Downarrow}/4L)\sum_{\vec{k},\vec{k}'}\vec{\sigma}_{\vec{k}}\cdot\vec{\sigma}_{\vec{k}'}$ and the drive $(\Omega/2)\sum_{\vec{k}}\hat{\sigma}_{\vec{k}}^z$. Both these terms conserve the total spin S, defined by $\vec{S}\cdot\vec{S}|S,M\rangle = S(S+1)|S,M\rangle$ where $\vec{S} = (\hat{S}^x, \hat{S}^y, \hat{S}^z)$, and $|S,M\rangle$ are collective-spin eigenstates with non-negative $S \in (L/2), (L/2) - 1, \ldots$ and projection $M \in S, S-1, \ldots, -S$ (satisfying $\hat{S}^z|S,M\rangle = M|S,M\rangle$). A spin-polarized initial state in the fully symmetric Dicke manifold $S = L/2$ will be confined to that manifold, as transitions to other manifolds induced by the kinetic terms will be energetically suppressed by the many-body gap [29,41,42]. This permits us to further simplify the Hamiltonian by projecting it into the Dicke manifold [34], yielding $\hat{H}_S \approx \hat{H}_{\text{OAT}}$, where

$$\hat{H}_{\text{OAT}} = -(U_{\Uparrow\Downarrow}/L)\vec{S}\cdot\vec{S} + \chi\hat{S}^z\hat{S}^z + \Omega\hat{S}^z. \qquad (11)$$

This is a one-axis twisting (OAT) model, which is well studied for its entanglement generation in the form of spin squeezing [43]. The coefficient χ is

$$\chi = \frac{1}{L-1}\frac{2(J_0 + J_1)^2 U_{\Uparrow\Downarrow}}{\Omega^2 - U_{\Uparrow\Downarrow}^2} - \frac{1}{L}(V_{ee} - 2V_{\Uparrow\Downarrow}). \qquad (12)$$
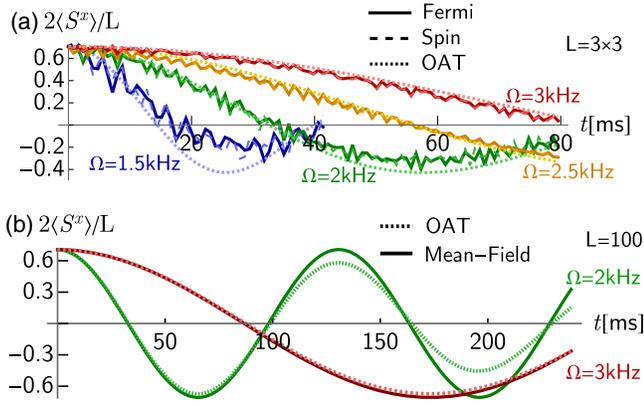
FIG. 3. (a) Time evolution of $\langle \hat{S}^x \rangle = C\cos(\phi)$ to measure the density phase shift ϕ, comparing the Fermi-Hubbard model + drive, $\hat{H}_{FH} + \hat{H}_\Omega$, spin model $\hat{H}_S$, and one-axis twisting model $\hat{H}_{OAT}$ for system size $L = 3 \times 3$ and inclination angle $\theta = \pi/4$. The parameters used lie along the purple dashed line in the previous Fig. 2(c). (b) Time evolution of $\langle \hat{S}^x \rangle$ for a larger system of $L = 100$, using only the OAT model together with its predicted mean-field behavior.

The first term comes from the tunneling, and the second from the nearest-neighbor interactions.

The coefficient χ can be measured using our Ramsey protocol through the phase shift ϕ. At the mean-field level, under the OAT model the collective spin rotates about the z axis of the Bloch sphere at a rate $\langle \hat{S}^+ \rangle = (L/2)e^{i\phi(t)}$, with $\phi(t) = 2\chi\langle \hat{S}^z \rangle t = \chi L \sin(\theta)t$ where $\langle \hat{S}^z \rangle = (L/2)\sin(\theta)$ is conserved. Figure 3(a) shows sample time evolutions of $\langle \hat{S}^x \rangle = \text{Re}[\langle \hat{S}^+ \rangle]$ with a tilt angle $\theta = \pi/4$ for both the OAT and the underlying Fermi-Hubbard and spin models. We see the expected oscillation with period set by $2\chi\langle \hat{S}^z \rangle$. In Fig. 3(b), we show the same dynamics for a larger system using only the OAT. The frequency of the oscillations is not very sensitive to system size since $\chi \sim 1/L$ and $\langle \hat{S}^z \rangle \sim L\sin(\theta)$. Since the amplitude of the oscillations is proportional to the contrast, which decays more slowly with increasing L, better visibility of the oscillations is possible in larger systems.

Conclusions and Outlook.—We have shown a robust and experimentally realistic protocol for observing long-sought p-wave physics in optical lattices. Our specific band configuration and laser dressing allows one to isolate the interaction dynamics via collective enhancement and see a signal on realistic timescales without the usual challenges of band relaxation or losses due to strong Feshbach resonance. The system can be reduced to a simple one-axis twisting model described by a single interaction parameter χ, which is straightforward to measure while capturing the dominant many-body p-wave effects.

While in this work we focus on simple dynamics probed via mean-field Ramsey spectroscopy, well controlled spin interactions such as OAT provide avenues to useful many-body entanglement generation and nonequilibrium quantum simulation. Further progress can realize more complex and interesting extended Fermi-Hubbard models [44] that are theoretically challenging and yet straightforward to implement in experiment using extensions of our basic scheme. This system also allows the exploration of noncollective physics, including pairing, the effects of vacancies, or local quantum correlations, using tools such as quantum gas microscopes already implemented in several state-of-the-art optical lattice experiments [45–49].

*Corresponding author.
mikhail.mamaev@colorado.edu

[1] C. Gross and I. Bloch, Science **357**, 995 (2017).
[2] F. Schäfer, T. Fukuhara, S. Sugawa, Y. Takasu, and Y. Takahashi, Nat. Rev. Phys. **2**, 411 (2020).
[3] V. Gurarie, L. Radzihovsky, and A. V. Andreev, Phys. Rev. Lett. **94**, 230403 (2005).
[4] V. Gurarie and L. Radzihovsky, Ann. Phys. (Amsterdam) **322**, 2 (2007).
[5] S. R. Elliott and M. Franz, Rev. Mod. Phys. **87**, 137 (2015).
[6] N. Read and D. Green, Phys. Rev. B **61**, 10267 (2000).
[7] J. Levinsen, N. R. Cooper, and V. Gurarie, Phys. Rev. Lett. **99**, 210402 (2007).
[8] H.-Y. Hui, P. Brydon, J. D. Sau, S. Tewari, and S. D. Sarma, Sci. Rep. **5**, 8880 (2015).
[9] Y. Jiang, D. V. Kurlov, X.-W. Guan, F. Schreck, and G. V. Shlyapnikov, Phys. Rev. A **94**, 011601(R) (2016).
[10] L. Yang, X. Guan, and X. Cui, Phys. Rev. A **93**, 051605(R) (2016).
[11] D. V. Kurlov, S. I. Matveenko, V. Gritsev, and G. V. Shlyapnikov, Phys. Rev. A **99**, 043631 (2019).
[12] M. Singh, S. Pilati, and G. Orso, Phys. Rev. A **102**, 053301 (2020).
[13] X. Li and W. V. Liu, Rep. Prog. Phys. **79**, 116401 (2016).
[14] Y. Tokura and N. Nagaosa, Science **288**, 462 (2000).
[15] P. Coleman, Heavy fermions: Electrons at the edge of magnetism, in *Handbook of Magnetism and Advanced Magnetic Materials* (John Wiley & Sons, Hoboken, 2007), https://dx.doi.org/10.1002/9780470022184.hmm105.
[16] M. A. Ruderman and C. Kittel, Phys. Rev. **96**, 99 (1954).
[17] M. Imada, A. Fujimori, and Y. Tokura, Rev. Mod. Phys. **70**, 1039 (1998).
[18] G. Khaliullin, Prog. Theor. Phys. Suppl. **160**, 155 (2005).
[19] M. Martin, M. Bishof, M. Swallows, X. Zhang, C. Benko, J. Von-Stecher, A. Gorshkov, A. Rey, and J. Ye, Science **341**, 632 (2013).
[20] B. DeMarco, J. L. Bohn, J. P. Burke, M. Holland, and D. S. Jin, Phys. Rev. Lett. **82**, 4208 (1999).
[21] C. A. Regal, C. Ticknor, J. L. Bohn, and D. S. Jin, Phys. Rev. Lett. **90**, 053201 (2003).

[22] C. Luciuk, S. Trotzky, S. Smale, Z. Yu, S. Zhang, and J. H. Thywissen, Nat. Phys. **12**, 599 (2016).

[23] I. B. Spielman, P. R. Johnson, J. H. Huckans, C. D. Fertig, S. L. Rolston, W. D. Phillips, and J. V. Porto, Phys. Rev. A **73**, 020702(R) (2006).

[24] T. Müller, S. Fölling, A. Widera, and I. Bloch, Phys. Rev. Lett. **99**, 200405 (2007).

[25] G. Wirth, M. Ölschläger, and A. Hemmerich, Nat. Phys. **7**, 147 (2011).

[26] T. Kock, M. Ölschläger, A. Ewerbeck, W.-M. Huang, L. Mathey, and A. Hemmerich, Phys. Rev. Lett. **114**, 115301 (2015).

[27] M. Di Liberto, A. Hemmerich, and C. Morais Smith, Phys. Rev. Lett. **117**, 163001 (2016).

[28] T. Hartke, B. Oreg, N. Jia, and M. Zwierlein, arXiv:2103.13992.

[29] A. M. Rey, L. Jiang, M. Fleischhauer, E. Demler, and M. D. Lukin, Phys. Rev. A **77**, 052305 (2008).

[30] L. Pricoupenko, Phys. Rev. Lett. **96**, 050401 (2006).

[31] Z. Idziaszek and T. Calarco, Phys. Rev. Lett. **96**, 013201 (2006).

[32] Z. Idziaszek, Phys. Rev. A **79**, 062701 (2009).

[33] N. T. Zinner, J. Phys. A **45**, 205302 (2012).

[34] See Supplemental Material, which includes Refs. [32,35,36], at http://link.aps.org/supplemental/10.1103/PhysRevLett .127.143401 for Notes A through F and Figs. S1 through S6.

[35] C. S. Chiu, G. Ji, A. Mazurenko, D. Greif, and M. Greiner, Phys. Rev. Lett. **120**, 243201 (2018).

[36] M. D. Swallows, M. Bishof, Y. Lin, S. Blatt, M. J. Martin, A. M. Rey, and J. Ye, Science **331**, 1043 (2011).

[37] S. Baier, M. J. Mark, D. Petter, K. Aikawa, L. Chomaz, Z. Cai, M. Baranov, P. Zoller, and F. Ferlaino, Science **352**, 201 (2016).

[38] C. Lhuillier and F. Laloë, J. Phys. France **43**, 197 (1982).

[39] A. Rey, A. Gorshkov, C. Kraus, M. Martin, M. Bishof, M. Swallows, X. Zhang, C. Benko, J. Ye, N. Lemke, and A. Ludlow, Ann. Phys. (Amsterdam) **340**, 311 (2014).

[40] M. Köhl, H. Moritz, T. Stöferle, K. Günter, and T. Esslinger, Phys. Rev. Lett. **94**, 080403 (2005).

[41] S. Smale, P. He, B. A. Olsen, K. G. Jackson, H. Sharum, S. Trotzky, J. Marino, A. M. Rey, and J. H. Thywissen, Sci. Adv. **5**, eaax1568 (2019).

[42] A. Chu, J. Will, J. Arlt, C. Klempt, and A. M. Rey, Phys. Rev. Lett. **125**, 240504 (2020).

[43] M. Kitagawa and M. Ueda, Phys. Rev. A **47**, 5138 (1993).

[44] O. Dutta, M. Gajda, P. Hauke, M. Lewenstein, D.-S. Lühmann, B. A. Malomed, T. Sowiński, and J. Zakrzewski, Rep. Prog. Phys. **78**, 066001 (2015).

[45] M. F. Parsons, F. Huber, A. Mazurenko, C. S. Chiu, W. Setiawan, K. Wooley-Brown, S. Blatt, and M. Greiner, Phys. Rev. Lett. **114**, 213002 (2015).

[46] E. Haller, J. Hudson, A. Kelly, D. A. Cotta, B. Peaudecerf, G. D. Bruce, and S. Kuhr, Nat. Phys. **11**, 738 (2015).

[47] L. W. Cheuk, M. A. Nichols, M. Okan, T. Gersdorf, V. V. Ramasesh, W. S. Bakr, T. Lompe, and M. W. Zwierlein, Phys. Rev. Lett. **114**, 193001 (2015).

[48] A. Omran, M. Boll, T. A. Hilker, K. Kleinlein, G. Salomon, I. Bloch, and C. Gross, Phys. Rev. Lett. **115**, 263001 (2015).

[49] G. J. A. Edge, R. Anderson, D. Jervis, D. C. McKay, R. Day, S. Trotzky, and J. H. Thywissen, Phys. Rev. A **92**, 063406 (2015).